



A survey of nuclear quadrupole deformation in order to estimate the nuclear MQM and its relative contribution to the atomic EDM

Searching for the best candidate to focus on an atomic EDM measurement: A nuclear physics perspective

Prajwal MohanMurthy¹ · Umesh Silwal² · Jeff A. Winger³

Accepted: 24 February 2024
© The Author(s) 2024

Abstract

Measurement of a non-zero permanent electric dipole moment (EDM) in fundamental particles, such as in an electron or a neutron, or in nuclei or atoms, can help us gain a handle on the sources of Charge-Parity (CP) violation, both in the Standard Model (SM) and beyond. The nuclear magnetic quadrupole moment (MQM), the central topic of this work, is also CP, P, and T violating. Nucleons and nuclei have a non-zero MQM from sources within the SM, but the nuclear MQM is dramatically enhanced if the nuclei are structurally quadrupole deformed. Multiple sources contribute to an atomic EDM namely: (i) nuclear EDM through its Schiff moment, which is enhanced by nuclear octupole deformation, (ii) CP violating interactions between the electrons and the nuclei, and (iii) the nuclear MQM that contributes to the atomic EDM in atoms with an unpaired valence electron. Our survey of nuclear quadrupole deformation identified 48 isotopes as ideal systems in which to search for a CP violating EDM via their enhanced nuclear MQM. Of these candidates, $^{223,225}\text{Fr}$, ^{223}Ra , $^{223,225,227}\text{Ac}$, ^{229}Th , and ^{229}Pa also have maximally enhanced nuclear Schiff moment contribution due to their octupole deformation. Laser cooling of the isotopes of Fr and Ra, among a few others, has already been demonstrated, making $^{223,225}\text{Fr}$ and ^{223}Ra some of the best systems in which to measure an EDM.

Keywords Nuclear moments · Fundamental symmetries · Electric dipole moment · Magnetic quadrupole moment · Nuclear structure

✉ Prajwal MohanMurthy
prajwal@alum.mit.edu
Jeff A. Winger
j.a.winger@msstate.edu

¹ Department of Physics, University of Chicago, Chicago, IL 60637, USA

² Department of Physics and Optical Science, University of North Carolina, Charlotte, NC 28223, USA

³ Department of Physics and Astronomy, Mississippi State University, Mississippi State, Jackson, MS P.O. Box 5167, 39762, USA

1 Introduction

We exist because of charge-parity (CP) violation! According to the three Sakharov conditions [1], the thus required baryon asymmetry of the universe demands: (i) baryon number violation, (ii) charge (C) and CP violation, and (iii) underlying interactions to be out of the thermal equilibrium. Remnant baryon and photon densities of the universe are remarkably well measured using the cosmic microwave background [2]. But the measured baryon asymmetry of the universe is nearly 8 orders of magnitude larger than that predicted by the Standard Model (SM) using sources of CP violation in the CKM-matrix [3]. This demands additional sources for baryonic CP violation.

Sub-atomic particles, like electrons and neutrons, as well as atoms can have large magnetic dipole moments [4]. Measurement of a permanent non-zero electric dipole moment (EDM) in subatomic particles and atoms, in addition to their non-zero magnetic dipole moment (MDM), is an indication of P, T, and CP violation. Table 1 indicates the effect of the discrete transforms of C, P, and T upon some relevant vector parameters of electric and magnetic fields, as well as electric and magnetic dipole moments. Even though the MDM is C and T odd, when taken in combination with the fact that the magnetic field is also C and T odd, it does not violate P, CP, or T. But EDM is not simultaneously odd and even with respect to the magnetic field, indicating P, CP, or T violation. Therefore, it is important to note that a permanent non-zero EDM in a particularly non-scalar system, one whose spin is non-zero, is key as a signature of P, CP, and T violation.

The only source of baryonic CP violation in the SM is within the CKM-matrix, which describes the weak interactions [5, 6]. This source of CP violation can be used to estimate the permanent EDM of neutrons and electrons: $d_n^{(CKM)} \approx 2 \times 10^{-32} \text{ e}\cdot\text{cm}$ [7] and $d_e^{(CKM)} \approx 5.8 \times 10^{-40} \text{ e}\cdot\text{cm}$ [8], respectively. No non-zero EDM of such particles has been measured yet. The current experimental upper bound on neutron and electron EDMs (at 90% C.L.) are $d_n < 1.8 \times 10^{-26} \text{ e}\cdot\text{cm}$ [9] and $d_e < 4.1 \times 10^{-30} \text{ e}\cdot\text{cm}$ [10]. However, strong interactions could also violate CP, via the Quantum-Chromo-Dynamics (QCD) $\bar{\theta}$ parameter [11]. There could also be mechanisms beyond the SM, like super-symmetry, that could add to these sources of CP violation [12]. Therefore, measuring a non-zero permanent EDM in subatomic particles or atoms, helps pin down the sources of CP violation, and aid in the search for additional sources of baryonic CP violation beyond the CKM-matrix. The estimates of EDMs of various systems within the SM, like that of neutrons, electrons and atoms, using sources of CP violation in the CKM-matrix and QCD- $\bar{\theta}$, have been well documented [13].

Atomic EDMs could arise from the EDM of nucleons and electrons, as well as CP violating interactions within the nucleus and between the electrons and nucleus [14]. An atomic EDM can also be generated by other CP violating electromagnetic moments of the nucleus, namely the magnetic quadrupole moment (MQM), being the lowest order such magnetic moment that could be non-zero [15]. The relative atomic EDM arising from the contribution of an enhanced nuclear Schiff moment, due to octupole and quadrupole deformations of the nucleus, was

Table 1 Effect of C, P, and T transforms on vector parameters of electric and magnetic fields and dipole moments

Vector parameter	\hat{P}	\hat{C}	\hat{T}
Electric Field (\vec{E})	−	−	+
Magnetic Field (\vec{B})	+	−	−
Electric dipole moment (\vec{d})	−	−	+
Magnetic dipole moment ($\vec{\mu}$)	+	−	−

previous surveyed and the isotopes of ^{221}Rn , $^{221,223,225,227}\text{Fr}$, $^{221,223,225}\text{Ra}$, $^{223,225,227}\text{Ac}$, ^{229}Th , and ^{229}Pa were identified as attractive candidates [16]. In this work, we have surveyed the quadrupole deformation of nuclei to identify candidate isotopes whose atomic EDM arising from the contribution of the nuclear MQM is maximally enhanced.

Many of these exotic and highly deformed isotopes can, for the first time, be produced in large numbers at the Facility for Rare Isotope Beams (FRIB). Furthermore, certain isotopes lend themselves to laser based cooling, owing to their atomic structure. Cooling can help increase the number density, and the measurable sensitivity to an atomic EDM. We present here new candidate isotopes, in light of the rates deliverable at FRIB, as well as laser cooling considerations.

2 Multipole expansion of the nuclear potentials

Writing the nuclear potentials in terms of a multipole expansion, lets us differentiate the nuclear electromagnetic moments from structure deformation, and also gives us a clue about the ground state nuclear spin that are apt for the measurement of the nuclear electromagnetic moments. A multipole expansion can be written for both the scalar and vector potentials [17], where the scalar potential, ϕ , is linked to the charge distribution, ρ , by $\phi(R) = 1/(4\pi\epsilon_0) \int d^3r \cdot \{\rho(r)/|R-r|\}$, and the vector potential, A , is linked to the current density, j , by $A(R) = \mu_0/(4\pi) \int d^3r \cdot \{j(r)/|R-r|\}$ ($\epsilon_0 = 8.8541878128(13) \times 10^{-12}$ F/m and $\mu_0 = 1.25663706212(19) \times 10^{-6}$ N/A² are the vacuum permittivity and permeability, respectively [4]). Here, the scalar potential satisfies $E = -\nabla\phi(R)$, while the vector potential satisfies $B = \nabla \times A(R)$, where E and B are electric and magnetic fields, respectively.

Both, scalar and vector potentials can be written as a sum of 2^l -pole moments. From the Purcell-Ramsey-Schiff theorem [18, 19], the nuclear scalar potential can be written as a Laplace expansion [20],

$$\phi(\mathbf{R}) = \frac{1}{4\pi\epsilon_0} \sum_{l=0}^{\infty} \frac{1}{R^{l+1}} \sum_{m=-l}^l (-1)^m Y_l^m(\hat{R}) \mathcal{Q}_l^m, \tag{1}$$

$$\mathcal{Q}_l^m = \sqrt{\frac{4\pi}{2l+1}} \int d^3r \cdot \rho(r) r^l Y_l^m\left(\frac{r}{r}\right), \tag{2}$$

where, \mathcal{Q}_l^m is the electric 2^l -pole moment, and Y_l^m are the spherical harmonics. In a rotationally symmetric system, when canonically considering the z-axis to be the direction along the spin, the only relevant multipole moment corresponds to $m = 0$. The nuclear charge, electric dipole moment (EDM: d), and electric quadrupole moment (EQM: Q), respectively, are given by [21]:

$$\mathcal{Q}_{l=0}^{m=0} = \int d^3r \cdot \rho(r) = Z_{\oplus}, \tag{3}$$

$$\mathcal{Q}_{l=1}^{m=0} = \int d^3r \cdot r \cos(\theta) \rho(r) = d, \tag{4}$$

$$\mathcal{Q}_{l=2}^{m=0} = \int d^3r \cdot r^2 (3 \cos^2(\theta) - 1) \frac{1}{2} \rho(r) = Q, \tag{5}$$

where Z is the atomic number of the nucleus, and e is the elementary charge. Similarly, the vector potential can be expanded as [22]:

$$A(R) = \frac{\mu_0}{4\pi} \sum_{l=0}^{\infty} \frac{1}{R^{l+1}} \sum_{m=-l}^l (-1)^m Y_l^m(\hat{R}) \mathcal{M}_l^m, \quad (6)$$

$$\mathcal{M}_l^m = \frac{1}{l+1} \sqrt{\frac{4\pi}{2l+1}} \int d^3r \cdot r^l Y_l^m\left(\frac{r}{r}\right) \cdot [\nabla \times j(r)], \quad (7)$$

where \mathcal{M}_l^m is the magnetic 2^l -pole moment. Along the lines of Eqs. 3-5, the magnetic monopole moment, magnetic dipole moment (MDM: μ), and magnetic quadrupole moment (MQM: M) terms can be written as [23]:

$$\mathcal{M}_{l=0}^{m=0} = 0, \quad (8)$$

$$\mathcal{M}_{l=1}^{m=0} = \int d^3r \cdot \frac{1}{2} r \times j(r) = \mu, \quad (9)$$

$$\mathcal{M}_{l=2}^{m=0} = \int d^3r \cdot \frac{1}{6} [(r \times j(r))r + r(r \times j(r))] = M. \quad (10)$$

A typical source for the origin of the nuclear current density, $j(r)$, is its spin, s .

It is important to note that the spherical harmonics are mutually orthogonal. Since the expectation value is proportional to the square of the wave function, cases where the wave function has a spherical harmonic term, $Y_{l=s}^m$, forces all terms involving $Y_{l>2s}^m$ in Eqs. 1 and 6 to zero. Accordingly, following the Wigner-Eckart theorem [24], from Eqs. 1-2 and 6-7, it can then be seen that nuclei with spin s , can have up to and including electromagnetic 2^{2s} -pole moments. Therefore we need at least a spin 1/2 nucleus to possess a non-zero EDM and MDM, and at least a spin 1 nucleus to possess a non-zero EQM and MQM.

Furthermore, it can be seen in Table 1 and its associated text, that in a nucleus with appropriately large MDM and non-zero spin, while EDM is CP violating, MDM obeys CP. Generalizing this along the lines of all electromagnetic 2^l -pole moments: electric $2^{2\mathcal{N}}$ -pole moments and magnetic $2^{2\mathcal{N}+1}$ -pole moments obey CP, and electric $2^{2\mathcal{N}+1}$ -pole moments and magnetic $2^{2\mathcal{N}}$ -pole moments violate CP, where \mathcal{N} is a whole number, $\mathcal{N} \in \mathbb{N}$. Therefore, electromagnetic moments like EDM (electric dipole ($2^{2(0)+1}$ -moment) and MQM (magnetic quadrupole ($2^{2(1)}$ -moment), in the context of quantifying CP violation, are extremely attractive [25]. In this work, we are concerned with nuclei that have a ground state spin of at least 1, so that we can study their CP violating permanent nuclear MQM, and its relative contribution to atomic EDM.

3 Nuclear Structure Deformation

The nucleus can be non-spherical. The deviation from the perfectly spherical geometry is successfully modeled using a rotationally symmetric two-fluid liquid drop model [26], each fluid corresponding to the ensemble of protons or neutrons [27]. The idea of an even-even core of the nucleus contributes significantly to the structure of the nucleus [21, 28], which also allows us to treat most other cases effectively as single particle systems. Following from the hydrodynamic origins of the liquid drop model [29–31], deformation in nuclei is also described in terms of 2^l -pole moments, similar to the electromagnetic moments in

Eqs. 2 and 7. The surface of a rotationally symmetric deformed nucleus can be described by [32–35]

$$R = c_V R_0 \left(1 + \sum_{l=2} \beta_l Y_l^{m=0} \right), \quad (11)$$

where $c_V = 1 - \{(1/\sqrt{4\pi}) \sum_{l=2} \beta_l^2\}$ is the volume normalization which ensures that the volume of the nucleus scales linearly with A regardless of the deformation, $R_0 = 1.2 \text{ fm} \cdot A^{1/3}$, A is the total number of nucleons in the nucleus, and β_l are the 2^l -pole structure deformation coefficients.

In Eq. 11, the imposition of rotational symmetry forces $m = 0$, similar to the reason we only considered electromagnetic moments in Eqs. 3–5 and 8–10 with $m = 0$. It must be noted that the connection between nuclear spin and the electromagnetic moments arising from the Wigner-Eckart theorem is not applicable to nuclear structure deformation, that is, even a spin-0 nucleus may and routinely does have deformations corresponding to $l \geq 2$ (making their $\beta_{l \geq 2} \neq 0$).

In this work, we have used structure deformation coefficients from the Möller-Nix model [36]. The Möller-Nix model is also based on the liquid drop model, but combines it with a folded Yukawa potential [37] in order to add shell model corrections using the Strutinsky method [38, 39]. With this combination, the Möller-Nix model is able to include the nucleon pairing effect [29], and most importantly, handle rotational degrees of freedom. The Möller-Nix model comprehensively provides deformation coefficients for all cases of even-even, even-odd, and odd-odd nuclei.

Examples of purely quadrupole and octupole deformed nuclei using Eq. 11 can be seen in Fig. 1 (Left) A and B, respectively. Here, for each of the two cases of quadrupole and octupole deformation, we have presented the shape of the nuclei for both positive (A-i: $\beta_2 = +0.3$, B-i: $\beta_3 = +0.2$) and negative (A-ii: $\beta_2 = -0.3$, B-ii: $\beta_3 = -0.2$) deformation coefficients. In the case of purely quadrupole deformed nuclei, Fig. 1 (Left) A-i and A-ii clearly demonstrate prolate and oblate shapes determined by the sign of the β_2 coefficient. In the case of purely octupole deformed nuclei, Fig. 1 (Left) B-i and B-ii clearly demonstrate the pear shapes determined by the β_3 coefficient. Since nuclei can be both quadrupole and octupole deformed simultaneously, we have also further shown a combination of prolate quadrupole deformation with both positive and negative octupole deformations in Fig. 1 (Left) C-i and C-ii, respectively.

Furthermore, we have plotted the β_2 and β_3 coefficient values from the Möller-Nix model in Fig. 1 (Right-Top) and (Right-Bottom), for the ground state of the isotopes, respectively. The collective behavior of both quadrupole and octupole deformation is clearly visible. Islands of quadrupole deformation are identifiable on either side of a magic number of nucleons, and the two major octupole deformation clusters, centered around $Z = \{56, 87\}$ and $N = \{89, 134\}$, are also visible. Canonically, the axis of symmetry in Fig. 1 (Left) A–C is also the axis of rotation. In case of non-zero spin, the spin vector sets the direction, where the positive direction is oriented along the same axis of symmetry. One of the poles, along the axis of symmetry, where the grid lines meet, is visible in each of these example deformed nuclei in Fig. 1 (Left). The predominance of prolate [over oblate] quadrupole deformation arises from quantum mechanics [40]. Combining this insight with the direction set by the spin, and considering that negative parity states (with opposite β_3) in octupole deformed nuclei arise from vibration of quadrupole deformed states, makes evident the fact that most octupole deformed nuclei are characterized by a negative β_3 [41]. Therefore, Fig. 1 (Left)

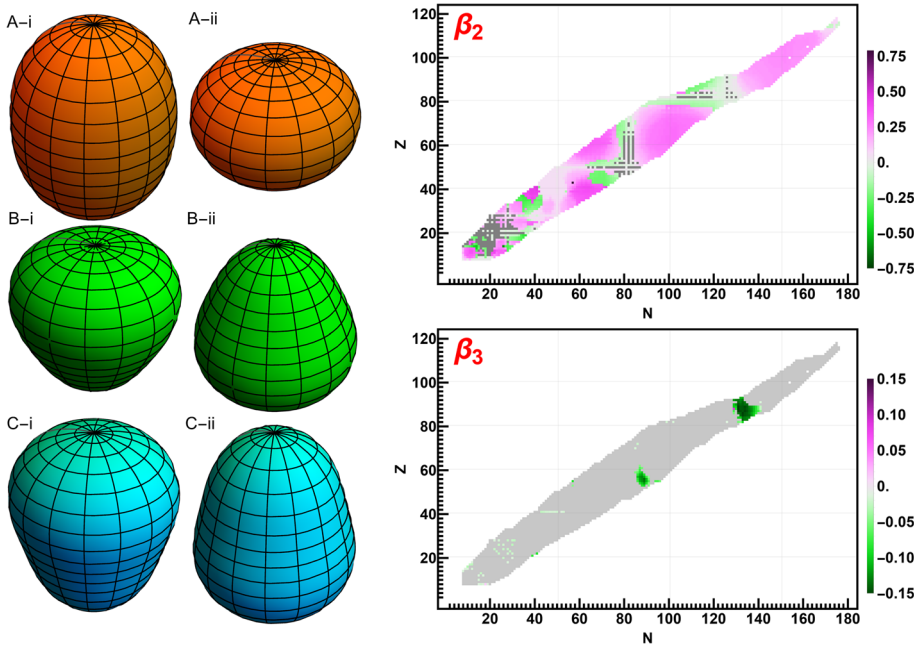


Fig. 1 [Left] Rendering of deformed nuclei - A: Quadrupole deformation (i: prolate, $\beta_2 > 0$; ii: oblate: $\beta_2 < 0$). B: Octupole deformation (i: $\beta_3 > 0$; ii: $\beta_3 < 0$). C: Prolate plus Octupole deformation (i: $\beta_2 > 0$, $\beta_3 > 0$; ii: $\beta_2 > 0$, $\beta_3 < 0$). [Right] Quadrupole (Top) and octupole (Bottom) deformation coefficients from the Möller-Nix model [36] for all isotopes whose binding energies are positive. Isotopes marked with light gray indicates that their binding energies are positive but their corresponding deformation is negligible

C-ii represents the most common ground state for each isotope with significant deformation seen in both Fig. 1 (Right-Top) and (Right-Bottom).

There are newer models which also calculate the deformation coefficients, for example *ref.* [42], which uses covariant density functional theory, and *ref.* [43], which combines a Skyrme Hartree-Fock model with Bardeen-Cooper-Schrieffer (BCS) type pairing. However, *ref.* [42] only handles even-even nuclei, whereas *ref.* [43] lacks comprehensive calculation of octupole deformation for relevant species. When available, these models predict deformation coefficients that are mutually consistent, within their model uncertainties [16].

4 Atomic electric dipole moment due to nuclear magnetic quadrupole moment

Typically, atomic EDMs are much smaller than nucleon EDMs, owing to the screening of the nuclear EDM by the electron cloud [19]. However, the electron screening is imperfect when [44]: (i) the valence electrons are highly relativistic, for example in paramagnetic atoms like ^{210}Fr [45]; (ii) the nucleus is heavily quadrupole and octupole deformed, *eg.* in diamagnetic atoms like ^{225}Ra [46]; or (iii) there are significant CP violating interactions between the electrons and the nucleus, *eg.* in diamagnetic atoms like ^{199}Hg [47]. The residual CP violating electromagnetic moment of a nucleus is usually referred to as the nuclear Schiff moment.

Furthermore, the nuclear MQM is not screened by the electron cloud, thereby dramatically increasing its relative contribution to the atomic EDM [48]. While the nuclear Schiff moment is enhanced by the simultaneous octupole and quadrupole deformations of the nucleus [21, 28, 46, 49], the nuclear MQM is enhanced by quadrupole deformation of the nucleus alone [50, 51].

Nuclear MQM arise from (i) intrinsic MQM of the constituent nucleons, (ii) the intrinsic EDM of the constituent nucleons in certain nuclear shells, and (iii) CP-violating interactions between the nucleons. Neutrons and protons, in addition to their intrinsic EDMs [7], also have intrinsic MQM, arising both from the CKM matrix as well as the QCD $\bar{\theta}$ [52]. An orbiting nucleon with an EDM also generates an MQM. This effect is particularly enhanced if the nucleus is quadrupole deformed, owing to the nucleon filling a nuclear shell which is tri-axially asymmetric [50, 52]. This is precisely captured in Eq. 12, where the nuclear MQM (and in turn the atomic EDM) is proportional to the quadrupole deformation, where β_2 also directly quantifies the deformation according to Eq. 11 [51]. Nuclear MQMs along with nuclear Schiff moments are also CP violating. In addition to the intrinsic nuclear EDM, the interaction of the nuclear MQM and the EDM of the electrons contributes to atomic EDM as well [52, 53]. In this section, we are only concerned with the approximate trends that dictate the enhancement of nuclear MQMs based on their quadrupole deformation, and their contribution to atomic EDMs, without explicitly calculating them, analogous to nuclear Schiff moments and their contributions to atomic EDMs in ref. [16]. The exact recipe for calculating MQMs of deformed nuclei is presented in refs. [50, 51].

The trends dictating the variation of nuclear MQMs as a function of nuclear quadrupole deformation (ref. [54], Section 10.3), and atomic EDM due to the nuclear MQM [15] are:

$$M \propto \beta_2 Z A^{2/3} ; d_{\text{atom}} \propto \frac{M Z^2}{E_+ - E_-} \implies d_{\text{atom}}^M \propto \frac{\beta_2 Z^3 A^{2/3}}{E_+ - E_-}, \tag{12}$$

where E_{\pm} are the energies of the ground state parity doublet. Even though ref. [54] (Section 10.3), indicates the trend $M \propto \beta_2 Z$, without the dependence on $A^{2/3}$, we have included this factor because the average rotational energy of a deformed nucleus follows the trend $\hbar\bar{\omega} \propto (45A^{-1/3} - 25A^{-2/3})$ [51, 55], which itself relies on the trend that $\beta_2 \propto A^{1/3}$ [54] (P. 197). The trends in Eq. 12 represent a relationship between electromagnetic moments, particularly the magnetic moments in Eqs. 8-10, to structure deformation coefficients in Eq. 11. These trends are sufficient to survey the nuclide chart, in order to study the quadrupole deformed systems in which atomic EDM is maximally enhanced.

5 Survey of nuclear quadrupole deformation

As a part of this survey, we considered: (i) quadrupole deformation, shown in Fig. 1 (Right-Top), (ii) ground state spins, shown in Fig. 2 (Top-Left), (iii) ground state parity doublet energy difference, shown in Fig. 2 (Bottom), (iv) decay lifetime, shown in Fig. 2 (Top-Right), and (v) stopped beam rates at FRIB, of 3176 isotopes whose binding energies are positive. For quadrupole deformation, we relied on the β_2 values in ref. [36]. For the binding energies, nuclear ground state spins, and decay lifetimes, we relied on the National Nuclear Data Center (NNDC) database [56], and for the isomers of isotopes and their associated energy levels in order to determine the ground state parity doublet energy difference, we

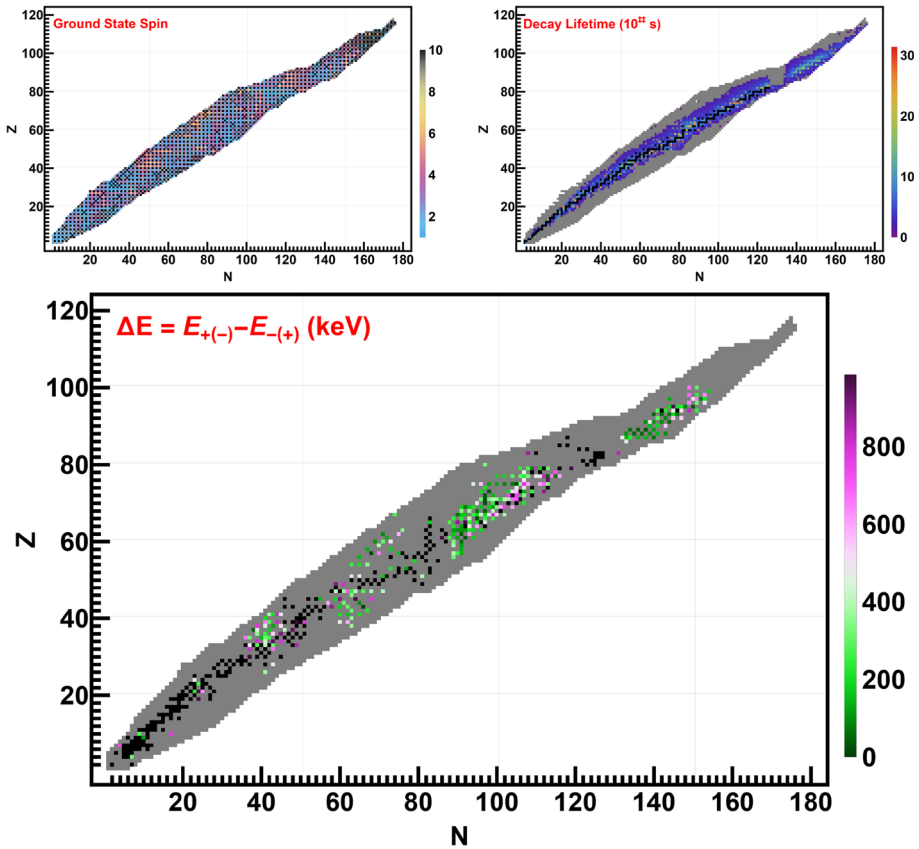


Fig. 2 [Top-Left] Ground state spin of nuclei with positive binding energy. Black and gray colors represent spin: $|s| = 0$ and spin: $|s| = 1/2$ species, respectively. [Top-Right] Ground state decay lifetime of nuclei with positive binding energy, where the lifetime is ≥ 1 minute, represented by colors corresponding to seconds in power of 10. [Bottom] Energy difference between the states that make up the ground state parity doublet in keV. Black represents that this energy difference is greater than 1 MeV, and gray represents that this energy difference has not been measured

used the International Atomic Energy Agency - Nuclear Data Services (IAEA-NDS) [57], both of which are based on ENSDF databases [58]. For the stopped beam rates at FRIB, we used the ultimate yields from LISE⁺⁺ [59].

In this survey, we are only concerned with the quadrupole deformation and the enhancement of the nuclear MQM due to it. Therefore, we only considered isotopes with a ground state nuclear spin greater than or equal to one, $j \geq 1$. We also only considered isotopes whose lifetimes are at least of the order of 1 minute, making it comparable to *ref.* [16]. Furthermore, according to Eq. 12, the nuclear MQM and the atomic EDM due to the nuclear MQM are proportional to the inverse of the ground state parity doublet energy difference, and therefore we only considered isotopes where this is lower than 1 MeV. Typically, the best candidates have a ground state parity doublet energy difference on the order of 10 keV [16].

The relative atomic EDMs follow the trend in Eq. 12: $d^M \propto \beta_2 Z^3 A^{2/3} / \Delta E_{\pm}$. We present this trend in Table 2, after normalizing them with that of ^{223}Ra , in order to keep it consistent with *ref.* [16]. Most experiments that measure EDMs in reality measure the precession frequency of the species by applying magnetic and electric fields, and employing the Ramsey technique of separated oscillating fields [18, 60, 61]. The measurement uncertainty associated with the EDM using the Ramsey technique scales as the square root of the number of particles, $\sqrt{W^{(\text{FRIB})}}$, where $W^{(\text{FRIB})}$ is the ultimate stopped beam rate achievable at FRIB. Ultimately, we are concerned with the combined impact of a highly enhanced MQM contribution according to Eq. 12, and access to a high experimental sensitivity. So we have also indicated this combined impact-factor, defined by $\mathcal{I} \propto \{\beta_2 Z^3 A^{2/3} / \Delta E_{\pm}\} \cdot \sqrt{W^{(\text{FRIB})}}$, in Table 2, after normalizing them against ^{223}Ra . Since atomic EDM due to nuclear MQM scales as $\propto Z^3$, heavy elements in this list are typically more impactful.

The isotope with the best relative atomic EDM, arising from its nuclear MQM enhanced by its quadrupole deformation, is ^{229}Pa . However, it is important to note that the level scheme for ^{229}Pa has not been adopted by NNDC, owing to the large relative uncertainty associated with the measurement of its ground state parity doublet energy difference of 0.06(5) keV [62]. The authors indicate that the existence of the ground state doublet in ^{229}Pa is uncertain. An earlier measurement by the same group had proposed the existence of a ground state doublet with an energy difference of 0.22(5) keV [63]; while another measurement indicating an energy difference of 99.3(4) keV [64] is also available. The next best candidate on our list in Table 2 is ^{245}Am . In Table 2, we have shown all candidate isotopes, which have a relative atomic EDM that are up to a factor of 10 lower than ^{245}Am . However, the beam rates for trans-Neptunium nuclei are not available in *ref.* [59]. We used the same LISE⁺⁺ toolkit [65–70] as in *ref.* [59], using a 5 kW - 177 MeV/u beam of ^{238}U incident on the FRIB production target [71, 72]. This new calculation of the beam rates, for the isotopes of $^{239,241,242,243,245}\text{Am}$ and ^{237}Pu , have also been presented in Table 2 and are highlighted in red. Even though isotopes of Americium, like other trans-Uranium isotopes, suffer from small rates at FRIB, an EDM experiment could potentially be conceived off the beam-line. We have presented certain isotopes that have a relative atomic EDM that is within a factor of 10 lower than ^{245}Am , but whose rates are below 0.1/day, in Table 3.

In Table 2, some isotopes have a lifetime of a few minutes, while others are on the order of many thousand years. Statistical precision of a measured EDM using the Ramsey technique of separated oscillating fields scales as the inverse of measurement time. The measurement time is usually restricted by the typical spin-coherence time in experiments on the order of a few minutes. Our choice of constraint, set to 1 minute on the decay lifetime, is long enough so that the factor coming from decay lifetimes can be comfortably left out.

Cooling and trapping the atoms and molecules helps achieve a high number density, increasing the statistical sensitivity of the measurement. Laser based cooling is one of the chief methods. It needs a (nearly) closed transition, which satisfies appropriate quantum selection rules like the $6S_{1/2}(F=4) - 6P_{3/2}(F=5)$ transition in Cesium, that can also be accessed by a commercially available laser, or in combination with secondary optics, like frequency doublers. Laser cooling has been traditionally demonstrated in alkali (Li, Na, K, Rb, Cs, Fr) and alkali-Earth (Mg, Ca, Sr, Ba, Ra [73]) atoms, as well as in Nobel gases (He, Ne, Ar, Kr, Xe) [74]. Similarly, transition metals (Hg, Ag, Cd, but also Cr), P-block elements (Al, Ga, In), f-block Lanthanides (Dy, Ho, Er, Tm, Yb), certain aspects of whose atomic structure are comparable to the traditional candidates, have also been laser cooled [74]. Atoms which have been laser cooled are particularly attractive to future work and have been highlighted in yellow in Table 2.

Table 2 Deformed nuclei whose production rates at FRIB are finite, with their relative theoretical expectation of EDM (d^M , Eq. 12), ultimate beam rate at FRIB ($W^{(FRIB)}$), and their relative impact-factor ($\mathcal{I} \propto d^M \sqrt{W^{(FRIB)}}$)

Z		$T_{1/2}$	β_2	j^π	ΔE (keV)	$ d^M $	$W^{(FRIB)}$	$\sim \mathcal{I} $
Z = 60	^{151}Nd	12.44(7) min	0.252	3/2 ⁺	57.6741(4)	0.34	4.06	0.12
Z = 61	^{153}Pm	5.25(2) min	0.270	5/2 ⁻	32.194(10)	0.70	3.58	0.24
Z = 62	^{153}Sm	46.284(4) hour	0.261	3/2 ⁺	35.844(3)	0.64	17.1	0.48
Z = 67	^{157}Ho	12.6(2) min	0.235	7/2 ⁻	66.911(20)	0.39	228	1.07
Z = 68	^{163}Er	75.0(4) min	0.272	5/2 ⁻	69.23(1)	0.47	56.3	0.64
	^{165}Er	10.36(4) hour	0.282	5/2 ⁻	47.159(4)	0.73	18.4	0.57
Z = 69	^{161}Tm	30.2(8) min	0.254	7/2 ⁺	78.20(3)	0.40	400	1.45
	^{168}Tm	93.1(2) day	0.294	3 ⁺	112(1)	0.34	21.3	0.28
Z = 70	^{167}Yb	17.5(2) min	0.274	5/2 ⁻	29.656(8)	1.23	164	2.86
Z = 72	^{169}Hf	3.24(4) min	0.274	5/2 ⁻	38.18(4)	1.05	599	4.66
Z = 73	^{171}Ta	23.3(3) min	0.255	(5/2 ⁺)	31.2(1)	1.26	710	6.09
	^{180}Ta	8.154(6) hour	0.269	1 ⁺	130.38(7)	0.33	88.3	0.56
Z = 75	^{173}Re	1.98(26) min	0.218	(5/2 ⁻)	118.1(12)	0.31	257	0.90
	^{175}Re	5.89(5) min	0.238	(5/2 ⁻)	125.3(1)	0.32	559	1.37
	^{177}Re	14(1) min	0.238	5/2 ⁻	84.70(10)	0.48	831	2.51

Table 2 continued

	$T_{1/2}$	β_2	j^π	$\Delta E(\text{keV})$	$ d^M $	$W^{(\text{FRIB})}$	$\sim Z $
^{179}Re	19.5(1) min	0.239	5/2 ⁺	65.35(9)	0.63	905	3.44
^{180}Re	2.46(3) min	0.248	1 ⁻	20.10(10)	2.13	852	11.28
$Z = 77$							
^{190}Ir	11.78(10) day	0.164	4 ⁻	36.154(25)	0.88	1480	6.14
^{192}Ir	73.829(11) day	0.145	4 ⁺	66.830(20)	0.42	1210	2.65
^{188}Au	8.84(6) min	-0.156	1(-)	82.70(8)	0.39	78.2	0.63
$Z = 79$							
^{223}Fr	22.00(7) min	0.146	3/2(-)	134.48(4)	0.34	3.60	0.12
^{225}Fr	3.95(14) min	0.163	3/2-	142.59(3)	0.36	0.92	0.06
$Z = 88$							
^{223}Ra	11.43(5) day	0.156	3/2 ⁺	50.128(9)	1.00	30.4	1.00
^{227}Ra	42.2(5) min	0.181	3/2 ⁺	90.0343(17)	0.65	3.40	0.22
^{229}Ra	4.0(2) min	0.189	5/2 ⁺	137.45(6)	0.45	0.68	0.07
^{231}Ra	103.9(14) s	0.207	(5/2 ⁺)	95.50(9)	0.71	69.2m	0.03
$Z = 89$							
^{223}Ac	2.10(5) min	0.147	(5/2 ⁻)	64.62(4)	0.76	152	1.70
^{225}Ac	9.920(3) day	0.164	(3/2 ⁻)	40.10(4)	1.37	84.4	2.28
^{227}Ac	21.772(3) year	0.172	3/2 ⁻	27.369(11)	2.11	38.7	2.38
^{229}Ac	62.7(5) min	0.189	(3/2 ⁺)	104.3(4)	0.61	13.6	0.41
$Z = 90$							
^{229}Th	7880(120) year	0.190	5/2 ⁺	146.3569(14)	0.45	136	0.95
^{231}Th	25.57(8) hour	0.198	5/2 ⁺	185.7160(13)	0.38	61.7	0.54
$Z = 91$							
$^{229}\text{Pa}^*$	1.50(5) day	0.190	(5/2 ⁺)	0.06(5)	1145	20.7	945

Table 2 continued

	$T_{1/2}$	β_2	j^π	$\Delta E(\text{keV})$	$ d^M $	$W^{(\text{FRIB})}$	$\sim Z $
$Z = 92$							
$Z = 93$							
^{231}Pa	$3.276(11) \times 10^4$ year	0.198	$3/2^-$	102.2685(21)	0.70	548	2.97
^{233}Pa	26.975(13) day	0.207	$3/2^-$	94.660(11)	0.80	359	2.75
^{235}Pa	24.4(2) min	0.215	$(3/2^-)$	51.79(17)	1.53	184	3.76
^{235}U	$7.04(1) \times 10^8$ year	0.215	$7/2^-$	81.724(4)	1.00	1610	7.28
$^{233}\text{Np}^*$	36.2(1) min	0.207	$(5/2^+)$	≈ 50	1.62	14.6	1.12
^{235}Np	396.1(12) day	0.215	$5/2^+$	49.10(10)	1.72	16.9	1.28
^{237}Np	$2.144(7) \times 10^6$ year	0.215	$5/2^+$	59.54092(10)	1.43	16.8	1.06
^{238}Np	2.099(2) day	0.215	2^+	182.8775(18)	0.47	15.8	0.34
^{239}Np	2.356(3) day	0.223	$5/2^+$	74.6640(10)	1.19	773m	0.19
$Z = 94$							
^{237}Pu	45.64(4) day	0.215	$7/2^-$	224.25(5)	0.39	31.0m	0.01
$Z = 95$							
^{239}Am	11.9(1) hour	0.215	$(5/2)^-$	187.1(5)	0.49	12.2 μ	0.31m
^{241}Am	432.6(6) year	0.223	$5/2^-$	205.883(10)	0.46	563n	62.6 μ
^{242}Am	16.02(2) hour	0.224	1^-	230.527(3)	0.42	1.21 μ	83.8 μ
^{243}Am	7364(22) year	0.224	$5/2^-$	84.00(16)	1.14	0.243 μ	0.11m
^{245}Am	2.05(1) hour	0.224	$5/2^+$	28.27(13)	3.45	3.88p	1.23 μ

Their relative theoretical expectation of EDM and their relative impact-factor, have both been normalized to ^{223}Ra . Their quadrupole deformation coefficients, β_2 , are from the Möller-Nix model [36]. Units of beam rate, $W^{(\text{FRIB})}$ is $10^6/\text{s}$ [65–70]. Parity doublet energy splitting, $\Delta E = E_- - E_+$, is in units of keV. *. Parity doublet energy levels have not been adopted by the National Nuclear Data Center (NNDC) database [56]

Table 3 Deformed nuclei whose production rates at FRIB are negligible, with the relative theoretical expectation for the EDM (d^M , Eq. 12)

		$T_{1/2}$	β_2	j^π	$\Delta E(\text{keV})$	d^M
$Z = 97$	^{241}Bk	4.6(4) min	0.224	$(7/2^+)$	128(7)	0.79
	^{249}Bk	330(4) day	0.235	$7/2^+$	82.599(13)	1.32
	^{250}Bk	3.212(5) hour	0.235	2^-	211.82(1)	0.52
$Z = 98$	^{249}Cf	351(2) year	0.235	$9/2^-$	243.13(7)	0.46
$Z = 99$	^{253}Es	20.47(3) day	0.236	$7/2^+$	181.3(5)	0.65

Their relative theoretical expectation for the EDM has been normalized to ^{223}Ra . Their quadrupole deformation coefficients, β_2 , are from the Möller-Nix model [36]. Parity doublet energy splitting, $\Delta E = E_- - E_+$, is in units of keV

6 Conclusion

The field of measuring EDMs in atoms is a thriving one with measurements already made in paramagnetic atoms of ^{89}Rb [75], ^{133}Cs [76], ^{171}Yb [77] and ^{205}Tl [78], and diamagnetic atoms of ^{199}Hg [79] and ^{129}Xe [80]. There is only one measurement made in an octupole deformed system: ^{225}Ra [73]. There are however proposals to measure the EDMs of ^{210}Fr [81] and ^{223}Rn [82]. Similarly, measurements in molecules also exist: HfF^+ [10], ThO [83], YbF [84], PbO [85], TlF [86], as well as proposals to make measurements in BaF [53], TaN [87], ThF^+ [88, 89], PbF [90–93], WC [94, 95], RaO [96, 97], RaF [98, 99], PtH^+ [100, 101], HgX [102], and FrAg [103]. Furthermore, in addition to the atoms where laser cooling has been achieved, molecules including MgF , AlF , CaF , SrF , YbF , BaF , RaF , TlF , BH , CH , BaH , AlCl , CaOH , SrOH , YbOH , and CaOCH_3 have also been laser cooled, paving the way for similar techniques being exploited in molecular systems [104].

It is important to note that the impact-factor, $\mathcal{I} (\propto \{\beta_2 Z^3 A^{2/3} / \Delta E_{\pm}\} \cdot \sqrt{W^{(\text{FRIB})}})$, in Table 2 is only relevant if one were to conceive of an in-beam EDM experiment at FRIB. However, the ^{225}Ra -EDM experiment [73] was an off-line measurement, using a stand alone source of ^{225}Ra atoms. Likewise the planned molecular experiments involving FrAg and RaAg [103] also plan to conduct an off-line measurement using a stand alone atomic beam source. Other considerations like the efficiency of their cooling and the cross-section with which these isotopes may form molecules with accessible transitions may dictate the relevant number density in these off-line measurements.

We here surveyed over 3176 isotopes, and particularly searched for candidates with the lowest energy difference between the states that make up their ground state parity doublet and highest quadrupole deformation. We thus arrived at 48 isotopes listed in Table 2 which are the most primed for a measurement of an atomic EDM, given their highly enhanced nuclear MQM and large production rates at FRIB. Similarly, we also identified the five trans-Uranium isotopes listed in Table 3 which are of interest, but would need to be produced at an alternate facility due to their negligible rates at FRIB. A similar study in *ref.* [16] surveyed the octupole deformations and identified a number of species among which are $^{223,225}\text{Fr}$, ^{223}Ra , $^{223,225,227}\text{Ac}$, ^{229}Th , and ^{229}Pa that overlap with the list presented here (Table 2). From Figs. 1 (Right-Top) and (Right-Bottom), the prevalence of quadrupole deformation compared with octupole deformation yields more candidate isotopes in this study of quadrupole deformation compared to the study in *ref.* [16]. Furthermore, laser cooling of 11 isotopes $^{163,165}\text{Er}$, $^{161,168}\text{Tm}$, ^{167}Yb , $^{223,225}\text{Fr}$, $^{223,227,229,231}\text{Ra}$ from the above list has already been demonstrated. Of all isotopes, the 3 isotopes $^{223,225}\text{Fr}$ and ^{223}Ra provide tantalizingly interesting

possibilities by the virtue of them having very close ground state parity doublets, maximal quadrupole and octupole deformation, as well as laser cooling already being demonstrated for them.

It was noted in *ref.* [16] that the deformation coefficients (in Fig. 1 (Right-Top) and (Right-Bottom)) sometimes differ by as much $\sim 50\%$, depending on the model of choice. This variation was also implicitly observed in this work. In this survey of 3176 isotopes, 90 isotopes had ground state spins which did not match the theoretical value, assuming the deformation shown in Fig. 1 (Right-Top) and (Right-Bottom). In such cases, we used the experimentally measured values. The relativistic term in Eq. 12 has been neglected here, and thereby depreciates the relative enhancement of nuclear MQM in heavier isotopes. But this source of uncertainty is typically less than that due to the variation in nuclear structure coefficients. Lastly, the level scheme has not been well established in many isotopes. This impacts our survey as well, particularly in the cases of ^{229}Pa and ^{233}Np , as indicated in Table 2. This work, especially in Eqs. 12, relies on relative factors that contribute to the nuclear MQM and in turn the atomic EDM. However, in order to capture the entirety of the effects that contribute to the nuclear MQM, ultimately a full calculation of nuclear deformation using a modified Nilsson model and based on *refs.* [50–53] is underway.

Acknowledgements We would like to thank J. Wacior for data transcription services.

Funding 'Open Access funding provided by the MIT Libraries'. One of the authors, P. M., would like to acknowledge support from Sigma Xi grants # G2017100190747806 and # G2019100190747806, US-Dept. of Education grant # F-19124368008, and US-Dept. of Energy grant #DE-SC0019768. P. M. and J. A. W. are supported by US-Dept. of Energy grant #DE-SC0014448.

Availability of data and materials Not applicable. There is no data beyond those represented in this manuscript.

Declarations

Ethical Approval Not applicable.

Conflicts of interest The authors declare that they have no conflict of interest.

Open Access This article is licensed under a Creative Commons Attribution 4.0 International License, which permits use, sharing, adaptation, distribution and reproduction in any medium or format, as long as you give appropriate credit to the original author(s) and the source, provide a link to the Creative Commons licence, and indicate if changes were made. The images or other third party material in this article are included in the article's Creative Commons licence, unless indicated otherwise in a credit line to the material. If material is not included in the article's Creative Commons licence and your intended use is not permitted by statutory regulation or exceeds the permitted use, you will need to obtain permission directly from the copyright holder. To view a copy of this licence, visit <http://creativecommons.org/licenses/by/4.0/>.

References

1. Sakharov, A.D.: Violation of CP-invariance, C-asymmetry, and baryon asymmetry of the universe. *JETP Lett.* **5**, 24 (1967). <https://doi.org/10.1070/PU1991v034n05ABEH00249>
2. Aghanim N., et al.: Planck 2018 Results -VI. Cosmological Parameters, *Astron. Astrophys. Suppl. Ser.* **641**, A6 (2020). <https://doi.org/10.1051/0004-6361/201833910>
3. Riotto, A., Trodden, M.: Recent progress in baryogenesis. *Annu. Rev. Nucl. Part. Sci.* **49**, 35 (1999). <https://doi.org/10.1146/annurev.nucl.49.1.35>
4. Tiesinga, E., Mohr, P.J., Newell, D.B., Taylor, B.N.: CODATA recommended values of the fundamental physical constants: 2018. *Rev. Mod. Phys.* **93**, (2021). <https://doi.org/10.1103/RevModPhys.93.025010>

5. Cabibbo, N.: Unitary symmetry and leptonic decays. *Phys. Rev. Lett.* **10**, 531 (1963). <https://doi.org/10.1103/PhysRevLett.10.531>
6. Kobayashi, M., Maskawa, T.: CP-Violation in the renormalizable theory of weak interaction. *Prog. Theoret. Phys.* **49**, 652 (1973). <https://doi.org/10.1143/PTP.49.652>
7. Khriplovich, I.B., Zhitnitsky, A.R.: What Is the value of the neutron electric dipole moment in the kobayashi-maskawa model? *Phys. Lett. B* **109**, 490 (1982). [https://doi.org/10.1016/0370-2693\(82\)91121-2](https://doi.org/10.1016/0370-2693(82)91121-2)
8. Yamaguchi, Y., Yamanaka, N.: Large long-distance contributions to the electric dipole moments of charged leptons in the standard model. *Phys. Rev. Lett.* **125**, (2020). <https://doi.org/10.1103/PhysRevLett.125.241802>
9. Abel, C., et al.: Measurement of the permanent electric dipole moment of the neutron. *Phys. Rev. Lett.* **124**, (2020). <https://doi.org/10.1103/PhysRevLett.124.081803>
10. Roussy, T.S., et al.: An Improved Bound on the Electron's Electric Dipole Moment. *Science* **381**, 46 (2023). <https://doi.org/10.1126/science.adg4084>
11. Hooft, G. 't.: Symmetry breaking through bell-jackiw anomalies, *Phys. Rev. Lett.* **37**, 8 (1976). <https://doi.org/10.1103/PhysRevLett.37.8>
12. Ellis, J.: Theory of the neutron electric dipole moment. *Nucl. Instrum. Methods Phys. Res. A* **284**, 33 (1989). [https://doi.org/10.1016/0168-9002\(89\)90243-X](https://doi.org/10.1016/0168-9002(89)90243-X)
13. Mohanmurthy, P., Winger, J. A.: Estimation of CP Violating EDMs from Known Mechanisms in the SM, Proc. of 40th International Conference on High Energy Physics (ICHEP2020) - PoS 390, p. 265 (2021). <https://doi.org/10.22323/1.390.0265>
14. Chupp, T.E., Fierlinger, P., Ramsey-Musolf, M.J., Singh, J.T.: Electric dipole moments of atoms, molecules, nuclei, and particles. *Rev. Mod. Phys.* **91**, (2019). <https://doi.org/10.1103/RevModPhys.91.015001>
15. Sushkov, O. P., et al.: *Possibility of Investigating P-and T-Odd Nuclear Forces in Atomic and Molecular Experiments*, *JETP Lett.* **60**, 873 (1984). www.osti.gov/biblio/5511886
16. Mohanmurthy, P., Silwal, U., Siwakoti, D.P., Winger, J.A.: Survey of deformation in nuclei in order to estimate the enhancement of sensitivity to atomic EDM. *AIP Conf. Proc.* **2249**, (2020). <https://doi.org/10.1063/5.0008560>
17. Jackson, J. D.: *Classical Electrodynamics*, 3rd Ed., Wiley-VCH (1998). ISBN: 0-471-30932-X. <https://ui.adsabs.harvard.edu/abs/1998clel.book.....J/abstract>
18. Purcell, E.M., Ramsey, N.F.: On the possibility of electric dipole moments for elementary particles and nuclei. *Phys. Rev.* **78**, 807 (1950). <https://doi.org/10.1103/PhysRev.78.807>
19. Schiff, L.I.: Measurability of nuclear electric dipole moments. *Phys. Rev.* **132**, 2194 (1963). <https://doi.org/10.1103/PhysRev.132.2194>
20. Griffiths, D. J.: *Introduction to Quantum Mechanics*, 2nd Ed., Pearson Prentice Hall (2004). <https://ui.adsabs.harvard.edu/abs/1995iqm.book.....G/abstract>
21. Spevak, V., Auerbach, N., Flambaum, V.V.: Enhanced T-Odd, P-Odd electromagnetic moments in reflection asymmetric nuclei. *Phys. Rev. C* **56**, 1357 (1997). <https://doi.org/10.1103/PhysRevC.56.1357>
22. Gray, C.G., Stiles, P.J.: Spherical Tensor Approach to Multipole Expansions. II. Magnetostatic Interactions. *Can. J. Phys.* **54**, 513 (1976). <https://doi.org/10.1139/p76-058>
23. Gray, C.G., Karl, G., Novikov, V.A.: Magnetic multipolar contact fields: the anapole and related moments. *Am. J. Phys.* **78**, 936 (2010). <https://doi.org/10.1119/1.3427412>
24. Hecht, K. T.: *The Wigner-Eckart Theorem*, Quantum Mechanics, Springer New York, NY (2000), pp. 299-302. https://doi.org/10.1007/978-1-4612-1272-0_32
25. Bernreuther, W., Suzuki, M.: The electric dipole moment of the electron. *Rev. Mod. Phys.* **63**, 313 (1991). <https://doi.org/10.1103/RevModPhys.63.313>
26. Bohr A., Mottelson, B.R.: *Collective and Individual Particle Aspects of Nuclear Structure*, Royal Danish Academy of Sciences and Letters 27, (1957). <https://inspirehep.net/literature/43880>
27. Bohr, A., Mottelson, B.R.: Rotational states in even-even nuclei. *Phys. Rev.* **90**, 717 (1953). <https://doi.org/10.1103/PhysRev.90.717.2>
28. Auerbach, N., Flambaum, V.V., Spevak, V.: Collective T- and P-Odd electromagnetic moments in nuclei with octupole deformations. *Phys. Rev. Lett.* **76**, 4316 (1996). <https://doi.org/10.1103/PhysRevLett.76.4316>
29. Weizsäcker, C.F.v.: *Zur Theorie Der Kernmassen*, *Zeitschrift Für Physik* **96**, 431 (1935). <https://doi.org/10.1007/BF01337700>
30. Bohr, N., Wheeler, J.A.: The mechanism of nuclear fission. *Phys. Rev.* **56**, 426 (1939). <https://doi.org/10.1103/PhysRev.56.426>
31. Gamow, G., Rutherford, E.: Mass Defect Curve and Nuclear Constitution, Proc. of the Royal Society of London 126, 632 (1997). <https://doi.org/10.1098/rspa.1930.0032>

32. Myers, W.D., Swiatecki, W.J.: Average nuclear properties. *Ann. Phys.* **55**, 395 (1969). [https://doi.org/10.1016/0003-4916\(69\)90202-4](https://doi.org/10.1016/0003-4916(69)90202-4)
33. Leander, G.A., Nazarewicz, W., Bertsch, G.F., Dudek, J.: Low-energy collective E1 mode in nuclei. *Nucl. Phys. A* **453**, 58 (1986). [https://doi.org/10.1016/0375-9474\(86\)90029-1](https://doi.org/10.1016/0375-9474(86)90029-1)
34. Nazarewicz, W.: Low-energy octupole and dipole modes in nuclei. *Nucl. Phys. A* **520**, c333 (1990). [https://doi.org/10.1016/0375-9474\(90\)91158-N](https://doi.org/10.1016/0375-9474(90)91158-N)
35. Butler, P.A., Nazarewicz, W.: Intrinsic dipole moments in reflection-asymmetric nuclei. *Nucl. Phys. A* **533**, 249 (1991). [https://doi.org/10.1016/0375-9474\(91\)90489-S](https://doi.org/10.1016/0375-9474(91)90489-S)
36. Möller, P., Nix, J.R., Myers, W.D., Swiatecki, W.J.: Nuclear ground-state masses and deformations. *At. Data Nucl. Data Tables* **59**, 185 (1995). <https://doi.org/10.1006/adnd.1995.1002>
37. Möller, P., Myers, W.D., Swiatecki, W.J., Treiner, J.: Nuclear mass formula with a finite-range droplet model and a folded-yukawa single-particle potential. *At. Data Nucl. Data Tables* **39**, 225 (1988). [https://doi.org/10.1016/0092-640X\(88\)90023-X](https://doi.org/10.1016/0092-640X(88)90023-X)
38. Strutinsky, V.M.: Shell effects in nuclear masses and deformation energies. *Nucl. Phys. A* **95**, 420 (1967). [https://doi.org/10.1016/0375-9474\(67\)90510-6](https://doi.org/10.1016/0375-9474(67)90510-6)
39. Strutinsky, V.M.: "Shells" in deformed nuclei. *Nucl. Phys. A* **122**, 1 (1968). [https://doi.org/10.1016/0375-9474\(68\)90699-4](https://doi.org/10.1016/0375-9474(68)90699-4)
40. Zickendraht, W.: Why are most nuclei prolate? *Ann. Phys.* **502**, 490 (1990). <https://doi.org/10.1002/andp.19905020607>
41. Butler, P.A.: Pear-shaped atomic nuclei. *Proc. Math. Phys. Eng. Sci.* **476**, 20200202 (2020). <https://doi.org/10.1098/rspa.2020.0202>
42. Agbemava, S.E., Afanasjev, A.V., Ring, P.: Octupole deformation in the ground states of even-even nuclei: A global analysis within the covariant density Functional Theory. *Phys. Rev. C* **93**, (2016). <https://doi.org/10.1103/PhysRevC.93.044304>
43. Ebata, S., Nakatsukasa, T.: Octupole deformation in the nuclear chart based on the 3D skyrme hartree-fock plus BCS model. *Phys. Scr.* **92**, (2017). <https://doi.org/10.1088/1402-4896/aa6c4c>
44. Liu, C.-P., Ramsey-Musolf, M.J., Haxton, W.C., Timmermans, R.G.E., Dieperink, A.E.L.: Atomic electric dipole moments: the schiff theorem and its corrections. *Phys. Rev. C* **76**, (2007). <https://doi.org/10.1103/PhysRevC.76.035503>
45. Engel, J., Ramsey-Musolf, M.J., van Kolck, U.: Electric dipole moments of nucleons, nuclei, and atoms: the standard model and beyond. *Prog. Part. Nucl. Phys.* **71**, 21 (2013). <https://doi.org/10.1016/j.pnpnp.2013.03.003>
46. Dzuba, V.A., Flambaum, V.V., Ginges, J.S.M., Kozlov, M.G.: Electric dipole moments of Hg, Xe, Rn, Ra, Pu, and Tl induced by the nuclear schiff moment and limits on time-reversal violating interactions. *Phys. Rev. A* **66** (2002). <https://doi.org/10.1103/PhysRevA.66.012111>
47. Chupp, T., Ramsey-Musolf, M.: Electric dipole moments: a global analysis. *Phys. Rev. C* **91** (2015). <https://doi.org/10.1103/PhysRevC.91.035502>
48. Flambaum, V.V., Murray, D.W., Orton, S.R.: Time invariance violating nuclear electric octupole moments. *Phys. Rev. C* **56**, 2820 (1997). <https://doi.org/10.1103/PhysRevC.56.2820>
49. Flambaum, V.V.: Enhanced nuclear schiff moment and time-reversal violation in 229Th-containing molecules. *Phys. Rev. C* **99**, (2019). <https://doi.org/10.1103/PhysRevC.99.035501>
50. Flambaum, V.V.: Spin hedgehog and collective magnetic quadrupole moments induced by parity and time invariance violating interaction. *Phys. Lett. B* **320**, 211 (1994). [https://doi.org/10.1016/0370-2693\(94\)90646-7](https://doi.org/10.1016/0370-2693(94)90646-7)
51. Lackenby, B.G.C., Flambaum, V.V.: Weak quadrupole moments. *J. Phys. G* **45**, (2018). <https://doi.org/10.1088/1361-6471/aac65d>
52. Lackenby, B.G.C., Flambaum, V.V.: Time reversal violating magnetic quadrupole moment in heavy deformed nuclei. *Phys. Rev. D* **98**, (2018). <https://doi.org/10.1103/PhysRevD.98.115019>
53. Flambaum, V.V., DeMille, D., Kozlov, M.G.: Time-reversal symmetry violation in molecules induced by nuclear magnetic quadrupole moments. *Phys. Rev. Lett.* **113**, (2014). <https://doi.org/10.1103/PhysRevLett.113.103003>
54. Khriplovich I.B., Lamoreaux, S.K.: CP Violation Without Strangeness: Electric Dipole Moments of Particles, Atoms, and Molecules, Springer Science & Business Media (2012). <https://inspirehep.net/record/460248>
55. Brown, B.A., Bertsch, G.F., Robledo, L.M., Romalis, M.V., Zelevinsky, V.: Nuclear matrix elements for tests of local lorentz invariance violation. *Phys. Rev. Lett.* **119**, (2017). <https://doi.org/10.1103/PhysRevLett.119.192504>
56. National Nuclear Data Center (NNDC). <https://www.nndc.bnl.gov/>. Accessed: Feb 1, 2023
57. International Atomic Energy Agency - Nuclear Data Services (IAEA-NDS). www-nds.iaea.org. Accessed: Feb 1, 2023

58. Evaluated and Compiled Nuclear Structure Data (ENSDF). <https://www.nndc.bnl.gov/ensdfarchivals/>. Accessed: Feb 1, 2023
59. FRIB Estimated Rates Version 2.10. <https://www.groups.nsl.msui.edu/frib/rates/fribrates.html>. Accessed: Feb 1, 2023
60. Ramsey, N.F.: A new molecular beam resonance method. *Phys. Rev.* **76**, 996 (1949). <https://doi.org/10.1103/PhysRev.76.996>
61. Ramsey, N.F.: A molecular beam resonance method with separated oscillating fields. *Phys. Rev.* **78**, 695 (1950). <https://doi.org/10.1103/PhysRev.78.695>
62. Ahmad, I., Chasman, R.R., Greene, J.P., Kondev, F.G., Zhu, S.: Electron capture decay of 58-min $^{229}_{92}\text{U}$ and levels in $^{229}_{91}\text{Pa}$. *Phys. Rev. C* **92**, (2015). <https://doi.org/10.1103/PhysRevC.92.024313>
63. Ahmad, I., Gindler, J.E., Betts, R.R., Chasman, R.R., Friedman, A.M.: Possible ground-state octupole deformation in ^{229}Pa . *Phys. Rev. Lett.* **49**, 1758 (1982). <https://doi.org/10.1103/PhysRevLett.49.1758>
64. Levon, A.I., et al.: The nuclear structure of ^{229}Pa from the $^{231}\text{Pa}(p, t)^{229}\text{Pa}$ and $^{230}\text{Th}(p, 2n)^{229}\text{Pa}$ reactions. *Nucl. Phys. A* **576**, 267 (1994). [https://doi.org/10.1016/0375-9474\(94\)90260-7](https://doi.org/10.1016/0375-9474(94)90260-7)
65. Tarasov, O., Bazin, D., Lewitowicz, M., Sorlin, O.: The code LISE: a new version for “Windows”. *Nucl. Phys. A* **701**, 661 (2002). [https://doi.org/10.1016/S0375-9474\(01\)01663-3](https://doi.org/10.1016/S0375-9474(01)01663-3)
66. Bazin, D., Tarasov, O., Lewitowicz, M., Sorlin, O.: The program LISE: a simulation of fragment separators. *Nucl. Instrum. Methods Phys. Res. A* **482**, 307 (2002). [https://doi.org/10.1016/S0168-9002\(01\)01504-2](https://doi.org/10.1016/S0168-9002(01)01504-2)
67. Tarasov, O.B., Bazin, D.: LISE++?: design your own spectrometer. *Nucl. Phys. A* **746**, 411 (2004). <https://doi.org/10.1016/j.nuclphysa.2004.09.063>
68. Tarasov, O.B., Bazin, D.: LISE++: exotic beam production with fragment separators and their design. *Nucl. Instrum. Methods Phys. Res. B* **376**, 185 (2016). <https://doi.org/10.1016/j.nimb.2016.03.021>
69. Tarasov, O.B., Bazin, D.: LISE++: radioactive beam production with in-flight separators. *Nucl. Instrum. Methods Phys. Res. B* **266**, 4657 (2008). <https://doi.org/10.1016/j.nimb.2008.05.110>
70. Kuchera, M.P., Tarasov, O.B., Bazin, D., Sherrill, B.M., Tarasova, K.V.: Plans for performance and model improvements in the LISE++ software. *Nucl. Instrum. Methods Phys. Res. B* **376**, 168 (2016). <https://doi.org/10.1016/j.nimb.2015.12.013>
71. Avilov, M., Fadeev, S., Fernandes, S., Golkovsky, M., Mittig, W., Pellemoine, F., Schein, M.: A 50-kW prototype of the high-power production target for the FRIB. *J. Radioanal. Nucl. Chem.* **305**, 817 (2015). <https://doi.org/10.1007/s10967-014-3908-1>
72. Pellemoine, F., Avilov, M., Mittig, W., Fernandes, S., Schein, M.: Development of a production target for FRIB: thermo-mechanical studies. *J. Radioanal. Nucl. Chem.* **299**, 933 (2014). <https://doi.org/10.1007/s10967-013-2623-7>
73. Bishof, M., et al.: Improved limit on the ^{225}Ra electric dipole moment. *Phys. Rev. C* **94**, (2016). <https://doi.org/10.1103/PhysRevC.94.025501>
74. McClelland, J.J., Steele, A.V., Knuffman, B., Twedt, K.A., Schwarzkopf, A., Wilson, T.M.: Bright focused ion beam sources based on laser-cooled atoms. *Appl. Phys. Rev.* **3**, (2016). <https://doi.org/10.1063/1.4944491>
75. Ensberg, E.S.: Experimental upper limit for the permanent electric dipole moment of Rb^{85} by optical-pumping techniques. *Phys. Rev.* **153**, 36 (1967). <https://doi.org/10.1103/PhysRev.153.36>
76. Murthy, S.A., Krause, D., Jr., Li, Z.L., Hunter, L.R.: New limits on the electron electric dipole moment from cesium. *Phys. Rev. Lett.* **63**, 965 (1989). <https://doi.org/10.1103/PhysRevLett.63.965>
77. Zheng, T.A., Yang, Y.A., Wang, S.-Z., Singh, J.T., Xiong, Z.-X., Xia, T., Lu, Z.-T.: Measurement of the electric dipole moment of ^{171}Yb atoms in an optical dipole trap. *Phys. Rev. Lett.* **129**, (2022). <https://doi.org/10.1103/PhysRevLett.129.083001>
78. Commins, E.D., Ross, S.B., DeMille, D., Regan, B.C.: Improved experimental limit on the electric dipole moment of the electron. *Phys. Rev. A* **50**, 2960 (1994). <https://doi.org/10.1103/PhysRevA.50.2960>
79. Graner, B., Chen, Y., Lindahl, E.G., Heckel, B.R.: Reduced limit on the permanent electric dipole moment of ^{199}Hg . *Phys. Rev. Lett.* **116**, (2016). <https://doi.org/10.1103/PhysRevLett.116.161601>
80. Allmendinger, F., Engin, I., Heil, W., Karpuk, S., Krause, H.-J., Niederländer, B., Offenhäusser, A., Repetto, M., Schmidt, U., Zimmer, S.: Measurement of the permanent electric dipole moment of the ^{129}Xe atom. *Phys. Rev. A* **100**, (2019). <https://doi.org/10.1103/PhysRevA.100.022505>
81. Inoue, T., et al.: Experimental search for the electron electric dipole moment with laser cooled francium atoms. *Hyperfine Interact.* **231**, 157 (2015). <https://doi.org/10.1007/s10751-014-1100-1>
82. Tardiff, E.R., et al.: The radon EDM apparatus. *Hyperfine Interact.* **225**, 197 (2014). <https://doi.org/10.1007/s10751-013-0898-2>
83. Collaboration, A.C.M.E., et al.: Order of magnitude smaller limit on the electric dipole moment of the electron. *Science* **343**, 269 (2014). <https://doi.org/10.1126/science.1248213>

84. Hudson, J.J., Kara, D.M., Smallman, I.J., Sauer, B.E., Tarbutt, M.R., Hinds, E.A.: Improved measurement of the shape of the electron. *Nature* **473**, 493 (2011). <https://doi.org/10.1038/nature10104>
85. Eckel, S., Hamilton, P., Kirilov, E., Smith, H.W., DeMille, D.: Search for the electron electric dipole moment using Ω -doublet levels in PbO. *Phys. Rev. A* **87**, (2013). <https://doi.org/10.1103/PhysRevA.87.052130>
86. Cho, D., Sangster, K., Hinds, E.A.: Search for time-reversal-symmetry violation in thallium fluoride using a jet source. *Phys. Rev. A* **44**, 2783 (1991). <https://doi.org/10.1103/PhysRevA.44.2783>
87. Skripnikov, L.V., Petrov, A.N., Mosyagin, N.S., Titov, A.V., Flambaum, V.V.: TaN molecule as a candidate for the search for a T, P-violating nuclear magnetic quadrupole moment. *Phys. Rev. A* **92**, (2015). <https://doi.org/10.1103/PhysRevA.92.012521>
88. Skripnikov, L.V., Titov, A.V.: Theoretical study of ThF^+ in the search for T, P-violation effects: effective state of a Th atom in ThF^+ and ThO compounds. *Phys. Rev. A* **91**, (2015). <https://doi.org/10.1103/PhysRevA.91.042504>
89. Loh, H., Cossel, K.C., Grau, M.C., Ni, K.-K., Meyer, E.R., Bohn, J.L., Ye, J., Cornell, E.A.: Precision spectroscopy of polarized molecules in an ion trap. *Science* **342**, 1220 (2013). <https://doi.org/10.1126/science.1243683>
90. Skripnikov, L.V., Petrov, A.N., Titov, A.V., Mawhorter, R.J., Baum, A.L., Sears, T.J., Grabow, J.-U.: Further investigation of G factors for the lead monofluoride ground state. *Phys. Rev. A* **92**, (2015). <https://doi.org/10.1103/PhysRevA.92.032508>
91. Petrov, A.N., Skripnikov, L.V., Titov, A.V., Mawhorter, R.J.: Centrifugal correction to hyperfine structure constants in the ground state of lead monofluoride. *Phys. Rev. A* **88**, (2013). <https://doi.org/10.1103/PhysRevA.88.010501>
92. Skripnikov, L.V., Kudashov, A.D., Petrov, A.N., Titov, A.V.: Search for parity- and time-and-parity-violation effects in lead monofluoride (PbF): ab initio molecular study. *Phys. Rev. A* **90**, (2014). <https://doi.org/10.1103/PhysRevA.90.064501>
93. McRaven, C.P., Sivakumar, P., Shafer-Ray, N.E.: Experimental determination of the hyperfine constants of the X_1 and a states of $^{207}\text{Pb}^{19}\text{F}$. *Phys. Rev. A* **78**, (2008). <https://doi.org/10.1103/PhysRevA.78.054502>
94. Lee, J., Meyer, E.R., Paudel, R., Bohn, J.L., Leanhardt, A.E.: An electron electric dipole moment search in the $X\ 3\Delta_1$ ground state of tungsten carbide molecules. *J. Mod. Opt.* **56**, 2005 (2009). <https://doi.org/10.1080/09500340903349930>
95. Lee, J., Chen, J., Skripnikov, L.V., Petrov, A.N., Titov, A.V., Mosyagin, N.S., Leanhardt, A.E.: Optical spectroscopy of tungsten carbide for uncertainty analysis in electron electric-dipole-moment search. *Phys. Rev. A* **87**, (2013). <https://doi.org/10.1103/PhysRevA.87.022516>
96. Flambaum, V.V.: Electric dipole moments of actinide atoms and RaO molecule. *Phys. Rev. A* **77**, (2008). <https://doi.org/10.1103/PhysRevA.77.024501>
97. Kudashov, A.D., Petrov, A.N., Skripnikov, L.V., Mosyagin, N.S., Titov, A.V., Flambaum, V.V.: Calculation of the parity-and time-reversal-violating interaction in ^{225}RaO . *Phys. Rev. A* **87**, (2013). <https://doi.org/10.1103/PhysRevA.87.020102>
98. Isaev, T.A., Berger, R.: Electron correlation and nuclear charge dependence of parity-violating properties in open-shell diatomic molecules. *Phys. Rev. A* **86**, (2012). <https://doi.org/10.1103/PhysRevA.86.062515>
99. Kudashov, A.D., et al.: Ab initio study of radium monofluoride (RaF) as a candidate to search for parity- and time-and-parity-violation effects. *Phys. Rev. A* **90**, (2014). <https://doi.org/10.1103/PhysRevA.90.052513>
100. Meyer, E.R., Bohn, J.L., Deskevich, M.P.: Candidate molecular ions for an electron electric dipole moment experiment. *Phys. Rev. A* **73**, (2006). <https://doi.org/10.1103/PhysRevA.73.062108>
101. Skripnikov, L.V., Petrov, A.N., Titov, A.V., Mosyagin, N.S.: Electron electric dipole moment: relativistic correlation calculations of the P, T-violation effect in the $3\Delta_3$ state of PbH^+ . *Phys. Rev. A* **80**, (2009). <https://doi.org/10.1103/PhysRevA.80.060501>
102. Prasanna, V.S., Vutha, A.C., Abe, M., Das, B.P.: Mercury monohalides: suitability for electron electric dipole moment searches. *Phys. Rev. Lett.* **114**, (2015). <https://doi.org/10.1103/PhysRevLett.114.183001>
103. Klos, J., Li, H., Tiesinga, E., Kotochigova, S.: Prospects for assembling ultracold radioactive molecules from laser-cooled atoms. *New J. Phys.* **24**, (2022). <https://doi.org/10.1088/1367-2630/ac50ea>
104. Fitch, N. J., Tarbutt, M. R.: Chapter Three - Laser-Cooled Molecules, *Advances In Atomic, Molecular, and Optical Physics*, Ed. L. F. Dimauro, H. Perrin, and S. F. Yelin, Acad. Press, vol. 70, pp. 157-262 (2021). <https://doi.org/10.1016/bs.aamop.2021.04.003>